Identification of a upstream transcription complex regulating miR-9 expression during neurogenesis

Diji Kuriakose
Monash University https://orcid.org/0000-0003-1067-7296
Fuad Iraqi
Tel Aviv University https://orcid.org/0000-0001-5525-206X
Grant Morahan
University of Western Australia https://orcid.org/0000-0002-8562-7325
Zhicheng Xiao (zhicheng.xiao@monash.edu)
Monash University https://orcid.org/0000-0001-5172-762X

Research Article

Keywords: miR-9, miRSome, CC mice, neuronal differentiation, histone modification, upstream regulation, chromatin loop, adult hippocampal neurogenesis

Posted Date: July 6th, 2022

DOI: https://doi.org/10.21203/rs.3.rs-1826909/v1

Abstract

MicroRNAs (miRs) are critical for many cellular processes, including neurogenesis. Little is known about the components of upstream regulation of miR. We studied regulation of miR-9, which is highly expressed in the brain. Using Collaborative Cross mice, significant quantitative trait loci (QTL) were mapped to regions containing 131 candidate genes. These were characterized by RNAi interference, qPCR and neuronal differentiation assays to derive a short list of candidates. Three of these encoded proteins (Panx2, Polr1c and Mgea5) were shown by ChIP-seq and Co-IP to associate mutually with each other and bind to the miR-9 locus. We named this DNA-protein interaction complex that acts upstream of miR-9, which serves as the site for regulating miRs' expression, “miRSome”. A 3C/ChIP-loop assay confirmed the chromatin organisation of the miRSome on the miR-9 locus. These results describe the components of upstream regulatory mechanism of miR-9 expression during neurogenesis.

Introduction

MicroRNAs (miRs) are small, 20–24bp long highly conserved, non-coding, single-stranded RNAs. miRs target many protein-coding genes and are involved in physiological processes such as cell proliferation, neuronal differentiation and apoptosis. miRs bind to target mRNAs and regulate their expression by either repressing translation or increasing mRNA degradation. Usually, the expression levels of miRs and their target gene(s) are inversely correlated [1]. Therefore, the role of miRs is crucial in regulating complex genetic networks and pathological pathways. However, we know little about upstream regulation of miRs. Coordinated transcriptional regulation of miRs is vital to enhance the robustness of gene regulation in mammalian genomes. Identifying the components – transcription factors, miRs, co-factors, accessory proteins, etc. – of this regulatory network is important to understand specific physiological and behavioural mechanisms, including underlying genes, signalling pathways, cells and tissues.

Certain miRs, such as miR-9, are highly expressed in the brain. The process of neurogenesis is highly conserved among vertebrates, and miRs modulate these processes differentially during various stages of neurogenesis [2]. miR-9-5p is located on mouse chromosome 7qD2 [3]. It is highly conserved in vertebrates and has two mature strands – miR-9-3p and miR-9-5p [4]. The predominant strand, miR-9-5p, is often called miR-9, whereas miR-9-3p, present at low levels, has been labelled miR-9*. In this paper, we focus on miR-9-5p, henceforth designated as miR-9. It plays a prominent role in cell proliferation and is critical for neurogenesis, triggering the transition to neuronal differentiation [5]. Key genes like *Tlx* [6], *Sirt1* [7] and *Bace1* [8] are direct downstream targets of miR-9. Dysregulation of miR-9 is linked to neurodegenerative disorders like Alzheimer’s disease (AD) [8], Huntington’s disease [9], Amyotrophic lateral sclerosis (ALS) [10] and Parkinson’s disease [7]. miR-9 hypermethylation has been reported in many tumours, hence it is also regarded as an epigenetically modified miR [11].

To identify upstream transcriptional regulator(s) of miR-9 during neurogenesis, we used the next-generation genetic resource, the Collaborative Cross (CC) [12]. The CC is a set of recombinant inbred mouse

strains derived from five classical strains (A/J, C57BL/6J, 129S1/SvlmJ, NOD/ShiLtJ, NZO/HlLtJ) and three wild–derived strains (CAST/EiJ, PWK/Ph, and WSB/EiJ). It captures over 90% of the common genetic diversity of the mouse species to maximize genetic mapping power and allow rapid identification of genes that control complex traits [13]. This study will focus on identifying the components of upstream regulation of miR-9 through CC mice.

Results

miR expression profiling data from CC mice maps QTL regions containing candidate regulatory genes

miR expression profiling data indicate genetic diversity in CC mice

Upstream regulation of miRs may involve multiple factor/s, so we needed to determine whether the CC was a suitable model for studying miR regulation. We performed qPCR expression analysis of three miRs: miR-9, miR-29a and miR-107. In brief, we utilized the hippocampi of male mice from 54 genetically diverse CC strains at two ages (5–6 weeks, and 30–40 weeks; **Table S1**). We found differential expression of miR-9, miR-29a and miR-107 between the CC strains. We observed an upregulation of 1.2±0.5 and downregulation of 0.65±0.17 in miR-9/29a/107 expression within the 5–6-week-old CC strains (**Figure 1A, Figures S1 A-B**). Similarly, we observed an upregulation of 5.1±2.7 and downregulation of 2.75±0.5 in miR-9/29a/107 expression within the 30–40-week-old CC strains used in this study (**Figure 1B, Figures S1 C-D**).

To further study diversity in gene expression between CC lines, we tested expression of the *Bace1* gene, a downstream target for miR-9/29a/107 [14; 15; 16]. Upregulation of miR should downregulate its targets, including *Bace1*, and vice versa. We checked whether in CC mice upregulation of miRs' expression downregulates *Bace1*. We observed this only for 50% CC strains in miR-9 whereas for 45% CC strains in miR-29a/107 in young mice hippocampus (**Figure 1C**). Similarly, for the hippocampus of older mice, only 63% CC lines in miR-29a and 53% in miR-9/107 respectively showed this change (**Figure 1D**). Therefore, these data confirm that CC mice offer the potential to identify upstream genetic factors in miR regulation.

QTL analysis and siRNA knockdown identify upstream candidates

The Gene Miner and HAPPY software packages were used to analyse miR expression data to map QTLs to specific genome locations. Here, we calculated the fold-change expression of miR-9/29a/107 and mapped the QTLs associated with this trait for each miR. We considered logarithm of the odds (LOD) scores >3 as significant to link the loci to the miR trait of interest. We identified QTLs on Chr 19 (LOD>3.78), Chr 15 (LOD>6.32), Chr 5 (LOD>4.24), Chr 7 (LOD>12.6), Chr 12 (LOD>11.2), Chr 17

(LOD>3.68), Chr 1 (LOD>12.5). QTLs were considered at the 50th and 95th percentile significance with a total of 131 genes resided within the mapped QTLs regulating miR-9/29a/107 expression (**Figures S1 E-J**). Of these genes, 40 were associated with the miR-9 regulatory QTL, 17 with the miR-29a QTL, and 88 were linked to the miR-107 QTL (**Table 1**).

In order to make a shortlist of the most promising candidates for further study, we short interfering RNAs (siRNAs) to knockdown the expression of all 131 genes individually (knockdown efficiency >70% was achieved, **Figures S1 K-L**). We performed this experiment using a mouse neuroblastoma cell line (Neuro-2a) and compared the fold-change (FC) regulation of miR-9/29a/107 to the scrambled siRNA negative control using qPCR (oligonucleotides listed in **Table S2**). We pooled the genes with FC>1 and identified 23 (of 131 candidates) that affected levels of miR-9/29a/107 (**Figure 1E**). Candidate gene prioritisation was performed employing a bioinformatics platform for gene ontology (GO) analysis and disease segregation. We used Enrichr, DAVID, DisGeNET and EBI to further reduce the candidate list by identifying modules enriched in processes related to neurogenesis, gene regulation and neurodegeneration. We also looked at the gene–disease association score to identify ontology classes related to neurodegenerative disorders (**Figures S1 M-N**). Thirteen (of 23) candidate genes – *Ahctf1, Mgea5, Polr1c, Trabd, Creld2, Lzts2, Mrpl14, Sccpdh, Pdcd11, Cuedc2, Ephx1, Nt5c2* and *Panx2* were matched to the desired GO terms (**Figure 1F**). Taken together, these experiments demonstrated that CC is a valuable tool for studying the genetic basis of miR regulation.

Panx2, Polr1c and *Mgea5* alter neuronal differentiation through miR-9 in mouse neural progenitor cells

Panx2, Polr1c and Mgea5 are involved in neuronal differentiation

miR-9 plays a prominent role in neuronal differentiation [5]. Therefore, in order to reduce the list of 13 candidate genes, we conducted a neuronal differentiation assay. Mouse neural progenitor cells (mNPCs) were isolated from the adult (30–40-week-old) mouse hippocampi to study the molecular mechanisms controlling hippocampal neurogenesis. To determine if the 13 candidate genes played any role in neuronal differentiation, mNPCs were treated with siRNAs for the 13 candidate genes, then allowed to differentiate for three days. Neuronal differentiation was quantified by the βIII-tubulin marker using Image J software. The number of βIII-tubulin positive cells changed significantly only after knockdown of four candidate genes, namely *Panx2, Polr1c, Mgea5* and *Ephx1* (**Figures S2 A-D**). *Panx2* increased, while both *Polr1c* and *Mgea5* decreased the number of neuronal-like cell phenotypes after knockdown (**Figures 2A-B**). *Ephx1* knockdown increased neuronal differentiation in mNPCs (**Figures S2 C-D**). To confirm these results, we performed rescue experiments to overexpress *Panx2*, *Polr1c* and *Mgea5* using a lentiviral system and determined if this reversed the effect of knockdown. We found that overexpression of *Panx2* in mNPCs decreased neuronal differentiation, whereas overexpression of *Polr1c* and *Mgea5* led to

increased neuronal differentiation compared to the effect of single knockdowns and control. (**Figures S2 E-H**). Therefore, *Panx2, Polr1c, Mgea5* and *Ephx1* were selected as the best candidates for further study.

-

miR-9 inhibition decreased neuronal differentiation

Since all the candidates identified resided in the QTL regions controlling miR-9/107 expression, we performed further study of the neuronal differentiation of miR-9/107 in mNPCs. We used miR inhibitors (miR-in) to inhibit miR function in mNPCs. After neuronal differentiation, we observed that miR-9-in reduced the number of βIII tubulin-positive cells significantly compared to the miR negative control (**Figures 2C-D**). miR-107 did not change neuronal differentiation significantly (**Figures S2 I-J**). To confirm the role of miR-9 in neuronal differentiation, we overexpressed miR-9 using lentivirus and found that neuronal differentiation was increased (**Figures S2 K-L**). These results demonstrate that miR-9 decreased neuronal differentiation in adult mNPCs.

-

Panx2, Polr1c and Mgea5 regulate neuronal differentiation through miR-9

To further test if *Panx2, Polr1c, Mgea5* and *Ephx1* altered neuronal differentiation through miR-9, we performed double knockdown experiments using siRNAs, together with miR-9-in. We found that neuronal differentiation was dramatically lower in *Panx2, Polr1c* and *Mgea5* than in the individual knockdowns and the scrambled negative control. However, *Ephx1*-transfected mNPCs did not show any significant change in neuronal differentiation after inhibition with miR-9 (**Figures S2 M-N**). Compared to the single knockdown of *Panx2*, double knockdown using siPanx2 and miR-9-in reduced 92% of the βIII tubulin-positive cells (**Figures 2E, F**). Similarly, double knockdown using siPolr1c and miR-9-in (**Figures 2E, G**), siMgea5 and miR-9-in (**Figures 2E, H**) decreased 57% and 80% of the βIII tubulin-positive cells, respectively. Furthermore, we tried to rescue the miR-9 mediated decrease in neuronal differentiation of *Panx2, Polr1c* and *Mgea5* by using miR-9 overexpressed lentiviral mNPCs. The knockdown of *Panx2* in miR-9 overexpressed mNPCs significantly increased 86% of βIII tubulin-positive cells (**Figures S2 O, P**). Similarly, miR-9-overexpressed mNPCs increased 89% and 53% of βIII tubulin-positive cells after knockdown using siPolr1c (**Figures S2 O, Q**) and siMgea5 (**Figures S2 O, R**) respectively. Thus, the miR-9-in-mediated decrease in neuronal differentiation of *Panx2, Polr1c* and *Mgea5* could be reversed by miR-9 overexpression. Overall, these data suggest that *Panx2, Polr1c* and *Mgea5* regulated neuronal differentiation through miR-9.

Distribution of the Panx2, Polr1c and Mgea5 binding peaks on the miR-9 locus

Panx2, Polr1c and Mgea5 proteins bind to the miR-9 locus

miR-9 is located within the 34kb long miR-9 host gene (miR-9hg) on chromosome 7. To determine how *Panx2, Polr1c* and *Mgea5* regulate miR-9 expression, we performed ChIP-seq (in duplicates) in mNPCs. The datasets were mapped to the miR-9 genomic locus using MACS3 software for peak calling. All three proteins encoded by these genes were found to have peaks enriched on the miR-9 locus in two independent ChIP-seq experiments. The ChIP-seq peaks were viewed using the Integrative Genomics Viewer [17]. Panx2 (**Figure 3A**), Polr1c (**Figure 3B**) and Mgea5 (**Figure 3C**) peaks are displayed in colour against the input control (shown in grey). Similarly, we performed ChIP-qPCR in wild-type mNPCs and validated the binding of Panx2, Polr1c and Mgea5 on the miR-9 genomic region (**Figure 3D,** oligonucleotides listed in **Table S2**). This experiment was compared using rabbit IgG as negative control, which showed no enrichment, and H3K4me3 (as positive control), which showed high enrichment on the miR-9 locus. Thus, our findings indicate that Panx2, Polr1c and Mgea5 bound to the miR-9 genomic locus.

In order to determine if the Panx2, Polr1c and Mgea5 binding regions were located on the regulatory region of miR-9, we examined whether they overlapped with cis-acting elements. Using the UCSC genome browser to identify the distribution of Encyclopedia of DNA Elements (ENCODE) sites and CpG islands, the region of interest overlapped with the sites that were highly enriched in ENCODE peaks and CpG islands (**Figures S3 A-C**). Therefore, these data suggest that Panx2, Polr1c and Mgea5 were recruited to the regulatory region of the gene encoding miR-9.

Panx2, Polr1c and Mgea5 binding sites correlate with acetylation

Acetylation of H3 at Lys9/14 is associated with transcriptionally active chromatin, whereas methylation at H3K9 is a hallmark for silent chromatin [18]. Histone mark H3K4me3 is also associated with higher transcriptional activity. We next examined the histone-specific modification of Panx2, Polr1c and Mgea5 binding sites on the miR-9 locus. Using ChIP-qPCR in wild-type mNPCs, we studied histone modification pattern of H3K4me3, H3K9/14ac, H3K9me2 and H3K9me3 on the 34kb locus of miR-9. We found that H3K9/14ac was predominantly enriched in all the binding sites of Panx2, Polr1c and Mgea5 on the miR-9 locus. We saw high enrichment of H3K4me3 in PoBS-1/2 and the miR-9 promoter region. MgBS2 also coincided with H3K9me3, which marks methylation. Overall, the level of acetylation was higher throughout the binding sites of Panx2, Polr1c and Mgea5 on the miR-9 locus in the wild-type mNPCs (**Figure 3E**).

Panx2, Polr1c and Mgea5 are associated with each other

In order to determine if Panx2, Polr1c and Mgea5 form a complex, we performed co-immunoprecipitation experiments (Co-IP). Wild-type mNPC lysates were individually immunoprecipitated with rabbit antibodies specific for each of Panx2, Polr1c and Mgea5 and probed using antibodies to the other two proteins. We used rabbit IgG (as negative control) and input control to confirm the specificity of the antibody. Polr1c and Mgea5-specific bands were found in the fraction immunoprecipitated with Panx2 antibody (**Figures 3F-G**). Mgea5 also precipitated Panx2 and Polr1c from mNPCs (**Figures 3H-I**). However, we did not observe any Panx2 and Mgea5-specific bands in the fraction immunoprecipitated with Polr1c antibody (possibly because anti-Polr1c binds an epitope that disrupts the interaction via steric interference or direct competitive binding) (**Figures 3J-K**). Thus, we demonstrated that Panx2/Mgea5 existed in a complex with each other and Polr1c. In this way, we determined an association between Panx2, Polr1c and Mgea5. A schematic of Co-IP interactions is shown in **Figure S3 D**.

Panx2, Polr1c and Mgea5 as a miRSome acting upstream of miR-9

Overall, we confirmed that Panx2, Polr1c and Mgea5 bind to the regulatory region of miR-9 locus and demonstrated a physical association with each other. We termed this intracellular complex, made of chromosomal DNA bound by the proteins, which serves as the site for regulating the expression of the gene encoding specific miR, called “miRSome”. The miRSome regulating miR-9 expression is referred to as “miR9Some”.

Nuclear signaling by *Panx2*, *Polr1c* and *Mgea5*

Cellular localization of Panx2, Polr1c and Mgea5

To further explore the functions of Panx2, Polr1c and Mgea5, we examined the localization of these three proteins as reported in the Uniprot protein database, that is, Panx2 in the cytoplasm, Polr1c in the nucleus and Mgea5 in both the cytoplasm and nucleus. To confirm this, we performed immunostaining in mNPCs using antibodies to Panx2, Polr1c and Mgea5. Panx2 was located in the cytoplasm, while Polr1c was localized to the nucleus. Mgea5 was present both in the nucleus and cytoplasm (**Figure S4 A**). Next, we performed immunoblotting in the cytoplasmic and nuclear extract using the respective antibodies. We found a 70KDa band in the cytoplasmic extract for Panx2, but this was absent from the nuclear extract. For Polr1c, a 40KDa band was identified in the nuclear extract, but was absent from the cytoplasm. In contrast, for Mgea5 a band at 130KDa was present in both the cytoplasmic and nuclear extracts (**Figures S4 B-D**).

Cleavage of Panx2 C-terminal fragment

Panx2 is a membrane protein with four transmembrane domains, two extracellular loops, one cytoplasmic N/C-terminal and one intracellular loop (**Figure 4A**). To determine whether the intracellular domain of Panx2 was cleaved and released from the cells, we performed a shedding assay. We tested the shedding of endogenous Panx2 from mNPCs, as well as from mNPCs stably expressing Panx2 protein. Western blot analysis of whole cell lysates using antibody directed against the C-terminal domain of Panx2 allowed detection of the cleaved C-terminal fragment (CTF). Panx2 CTF migrated as a lower molecular weight fragment than the full-length Panx2 (70KDa). The cleavage of membrane proteins can be increased by agents that activate protein kinase C [19]. In order to investigate if Panx2 cleavage was mediated by a similar mechanism, we used phorbol ester PMA, which is an activator of protein kinase C. mNPCs were treated with PMA for 2 hours at 37^{o}C, and this resulted in an increased Panx2 CTF. We detected the presence of two fragments that were enriched after PMA treatment, which we termed CTF25 and CTF17 (**Figure 4B**). We also detected CTF25/CTF17 in mNPCs stably expressing Panx2, and overall showed a similar pattern as endogenous Panx2 as detected by the western blot analysis (**Figure 4C**). We transfected Panx2 CTF into mNPCs and found enrichment of CTF25/CTF17 fragments (**Figure 4D**). We also tested the effect of inhibition on the cleavage of Panx2 using DAPT (γ-secretase inhibitor) and metalloprotease inhibitor GM6001. The presence of either agent reduced the levels of CTF25/CTF17 compared to the PMA treatment alone but was the same as treatment with the vehicle (DMSO) (**Figures 4B-D**). Overall, these data suggested that Panx2 cleavage was mediated by PMA and γ-secretase/metalloprotease inhibitors, similar to other membrane proteins [20; 21; 22; 23]. Finally, we identified a nuclear localization signal (NLS) in the CTF (amino acid: 341-343) of Panx2. We transfected the mutated NLS Panx2 c-terminal fragment into mNPCs and, using western blotting, found that CTF25/CTF17 was not formed at all (**Figure 4E**).

Nuclear translocation of Panx2

Next, we determined whether the cleaved Panx2 would be translocated to the nucleus. We treated mNPCs with PMA followed by nuclei isolation and immunoprecipitation with antibody to the Panx2 c-terminal domain or control rabbit IgG. There was a drastic increase in the levels of CTF25 relative to the control. Upon overexposure, we also detected CTF17 in the nucleus (**Figure 4F**). To visualize endogenous Panx2 in the nucleus, we stained the mNPCs under experimental conditions (unstimulated, PMA treatment, mutated Panx2-CTF-△341-343 and vehicle) with Panx2 c-terminal antibody. We saw higher nuclear signals in the PMA treated mNPCs than in the controls (**Figure 4G and Figures S4 E**).

We also analyzed the cellular localization of endocytosed CTF by performing live antibody uptake experiments. mNPCs incubated with Panx2 antibody (directed against the c-terminal fragment) at 4^{o}C (to prevent endocytosis) showed surface labelling of cells. Following binding, the cells were incubated at 0

minutes or 2 hours at 37°C after PMA treatment. At 0 minutes, the antibody was still surface bound, but after 2 hours, the vast majority of the surface-bound antibody was endocytosed and translocated to the nucleus. The DMSO vehicle was sued as a treatment control with only secondary antibody to rule out non-specific binding (**Figure S4 F**). We also performed live cell imaging using a similar method to determine if the surface-bound CTF Panx2 antibody was transported to the nucleus. PMA-treated Panx2 showed internalization into the nuclear region (**Figure S4 Movie G**), whereas the control remained unaffected (**Figure S4 Movie H**). These results suggest that Panx2 was cleaved and the CTF was transported to the nucleus.

Panx2, *Polr1c* and *Mgea5* regulate a chromatin-associated loop of the miR-9 locus

Panx2, Polr1c and Mgea5 form chromatin associated loop across miR-9 locus

Next, we explored the potential role of the miR9Some in higher-order chromatin loop organization in the 34kb miR-9 locus (**Figure 5A**). We hypothesized that if two or more remote sequences are physically close to each other, they may be confined to the same restriction enzyme-digested fragments of the crosslinked chromatin. Two candidate gene binding site (CGBS) sequences were extracted from *Panx2*, *Polr1c* and *Mgea5* binding on the miR-9 genomic region as determined by the ChIP-seq data. We designed CGBS-specific primers to test if any of the binding sites were brought near each other (oligonucleotides listed in **Table S2**). If they were trapped in the same fragment, then it could be ligated and amplified by qPCR. To determine the loop, we used a chromosome conformation capture (3C) assay on crosslinked chromatin [24]. We also used a ChIP-loop assay, which combines the 3C assay and immunoprecipitation with a specific antibody. This method helped to reveal the *Panx2*, *Polr1c* and *Mgea5*-specific loops and understand the histone-specific modifications related to transcriptionally active chromatin state associated with acetylation or transcriptionally silent chromatin configuration linked to methylation. We detected amplified signals using the primer sets F2 and F4 in the *Panx2*/*Polr1c* immunoprecipitated chromatin. The F2–F4 combination gave rise to an 8.4kb loop at the miR-9 locus. We detected a similar 8.4kb F2-F4 associated loop on the crosslinked chromatin isolated from the wild-type mNPCs without immunoprecipitation (3C assay). In contrast, this loop was not formed on the chromatin isolated from *Panx2*/*Polr1c*-null chromatin (**Figures 5B-C,** red box). Another 11.2kb loop was detected in the chromatin isolated from *Mgea5* null mNPCs by the primers F3-F5. This loop was also seen after immunoprecipitation with *Mgea5* antibody in the *Mgea5* null mNPCs. But the wild-type mNPCs immunoprecipitated with *Mgea5* antibody and wild-type mNPCs (3C assay) did not show the F3–F5 mediated 11.2kb loop (**Figure 5D,** magenta box). These data indicate that *Panx2*/*Polr1c* organised the chromatin into an 8.4kb loop, whereas *Mgea5*-null organised the chromatin into an 11.2kb loop of the miR-9 locus.

Panx2/Polr1c chromatin represents active chromatin and Mgea5 null chromatin represents silent chromatin

Next, we performed a ChIP-loop assay on the chromatin isolated from wild-type and *Panx2*/*Polr1c*/*Mgea5* null mNPCs after immunoprecipitation with antibodies against acetylated H3-Lys9/Lys14 and dimethylated H3-Lys9. Using acetylated H3-Lys9/Lys14, we detected an 8.4kb F2-F4 loop on the wild-type mNPCs (**Figure 5E**, red box). We specifically detected the 11.2kb loop using the dimethylated H3-Lys9 in the Mgea5 null mNPCs (**Figure 5F**, blue box). The 8.4kb loop was closely associated with the miR-9 promoter and showed the enrichment of acetylation, whereas the 11.2kb loop was formed away from the miR-9 promoter region and was methylated. Therefore, the 8.4kb loop represented the transcriptionally active chromatin state and the 11.2kb loop formed the transcriptionally silent chromatin.

A Bacterial Artificial Chromosome (BAC) clone (RP23-207N5) containing the 34kb miR-9 locus was used to test the primer sets and normalize the PCR data (**Figure 5G**). Non-immune serum and genomic DNA were used as negative controls (**Figures 5H-I**). C1 and C2 were used as internal primer controls. A1 and A2 indicate PCR products derived from β-actin locus primers (**Figure 5J**).

Overall, according to our data, the higher-order chromatin structure was mediated by Panx2/Polr1c/Mgea5 binding to the miR-9 locus. A model based on our data is shown in **Figure 5K**. *Panx2* and *Polr1c* mediated the 8.4kb loop at the miR-9 promoter and represented the active chromatin marked by acetylation. *Mgea5* mediated the 11.2kb loop and depicted the silent chromatin marked by methylation. These data confirm that the long-range interactions formed by the miR9Some forms the miR-9 genomic region into a chromatin loop structure.

The miR9Some acts upstream to regulate miR-9 expression and drives neuronal differentiation

The miR9Some regulates miR-9 expression

We determined how the miR9Some regulates miR-9 expression in wild-type mNPCs and in *Panx2*-, *Polr1c*-, *Mgea5*- null mNPCs. There was a basal level of miR-9 expression in wild-type mNPCs, while miR-9 expression increased (approximately 1.5-fold change) in the individual *Panx2*/*Polr1c*/*Mgea5* null mNPCs

(**Figure 6A**). Next, we tested the combined effect of the miR9Some on miR-9 expression. We knocked down all three miR9Some genes in mNPCs and found that expression of miR-9 increased dramatically (approximately a threefold change) compared to the wild-type mNPCs and individual *Panx2*-, *Polr1c*- and *Mgea5*- null mNPCs (**Figure 6B**). To confirm that the miR9Some was essential to trigger luciferase activity in miR-9 promoter, we transfected *Panx2*, *Polr1c* and *Mgea5* siRNAs with miR-9 and a mutant miR-9 lentiviral system in mNPCs. We found that *Panx2*, *Polr1c* and *Mgea5* strongly triggered luciferase activity. The luciferase activity of miR-9 promoter was significantly increased upon downregulation of individual *Panx2*, *Polr1c*, *Mgea5* and miR9Some compared to the miR-9 wild-type and scrambled negative control (**Figure 6C**). In the mutant miR-9 promoter, luciferase activity was unchanged (**Figure 6D**). Taken together, these data suggest that miR9Some upregulated miR-9 transcription by directly binding to the miR-9 promoter.

A regulatory pathway comprising miR9Some, miR-9 and Bace1

Bace1 is a downstream target of miR-9. We hypothesized that miR9Some should affect *Bace1* expression in the same way as for miR-9, because miR-9 targets *Bace1*. We measured *Bace1* expression in wild-type mNPCs, individual *Panx2, Polr1c, Mgea5* null mNPCs and miR9Some null mNPCs and found that *Bace1* levels were increased in individual *Panx2-, Polr1c-* and *Mgea5-* null mNPCs compared to the wild-type mNPCs (approximately 1.5-fold change) (**Figure 6E**). Furthermore, the miR9Some-null mNPCs showed approximately 30% greater reduction in the levels of *Bace1* than in mNPCs with individual knockdown of *Panx2, Polr1c* and *Mgea5*. Next, we compared the expression of *Bace1* and miR-9 after miR9Some knockdown and found reduction in *Bace1* expression was probably due to increased miR-9 expression (**Figure 6F**). These results demonstrated that miR9Some regulated the expression of both miR-9 and *Bace1* forming a regulatory pathway.

miR9Some acts in synergy to modulate neuronal differentiation

Because the miR9Some regulates miR-9 expression, we questioned whether it synergistically modulates neuronal differentiation of mNPCs. To perform this experiment, we generated mNPCs with different combinations of the double and triple knockdown cells *Panx2/Polr1c*, *Panx2/Mgea5, Polr1c/Mgea5*, miR9Some and each of these alongside miR-9-in. All the above experimental conditions were compared to the individual *Panx2, Polr1c and Mgea5* null mNPCs. We quantified the number of βIII tubulin-positive cells to determine neuronal differentiation. *Panx2* knockdown showed a higher increase in neuronal differentiation than all other experimental conditions (**Figure 6G and Figure S5 A**). The increase in neuronal differentiation was mainly mediated by *Panx2* and *Mgea5*. In *Polr1c* null mNPCs, *Panx2* and *Mgea5* increased the βIII tubulin-positive cells significantly compared to the single *Polr1c* knockdown (**Figure 6H and Figure S5 A**). In *Mgea5* null mNPCs, we observed a *Panx2*-mediated increase in neuronal differentiation of mNPCs compared to the single *Mgea5* knockdown (**Figure 6I and Figure S5 A**). The

miR9Some knockdown also showed increased neuronal differentiation. Likewise, miR9Some in combination with miR-9-in did not significantly decrease neuronal differentiation (**Figures 6G-I**). These experiments suggest that the miR9Some knockdown increased neuronal differentiation.

Discussion

The gene regulatory network controlling miR regulation is not well understood. In this study, we defined some components of this regulatory network; these components form a complex comprised of DNA and protein we dub a “miRSome”, that regulate expression of miRs. Specifically, we explored the transcriptional regulation of miR-9 during neurogenesis through miR9Some, involving an intracellular complex formed of Panx2, Polr1c and Mgea5, which binds to the miR-9 genomic locus marked by acetylation and methylation. The miR9some makes a chromatin loop along the miR-9 locus, regulating the expression of miR-9 and its downstream target *Bace1* during adult hippocampal neurogenesis (**Figure 7**).

-

A holistic approach to identifying candidates

The mouse animal models for studying neurodevelopmental disorders (NDDs) mostly rely on one strain and a single genetic background. Research on AD and ALS has shown that genetic variation can contribute significantly to disease phenotype variation [25; 26]. Therefore, our rationale was to use a genetically diverse mouse model to provide better power to establish a relationship between phenotype and genotype. CC mice offer great genetic diversity and corresponding phenotypic diversity in a wide range of traits, including NDDs [26]. Using miR-9/29a/107 expression profiling (**Figure 1**), we confirmed that the CC shows diversity in this trait. We mapped relevant QTLs associated with miR-9/29a/107 expression. *Panx2* and *Mgea5* reside within the miR-9 QTL, while *Polr1c* is within the miR-107 QTL (No candidate genes from the miR-29a QTL region were found significant, perhaps we will increase the strength of the CC mice to find the significant genes). miR-107 is a global regulator of miRs by controlling Dicer expression, so it must also affect miR-9 expression [27]. Therefore, we reasoned that the three genes *Panx2*, *Polr1c* and *Mgea5* all contribute to the regulation of miR-9. *Panx2*, *Polr1c* and *Mgea5* were indeed shown to regulate miR-9 expression and were identified as key players in neuronal differentiation.

Nuclear localisation of Panx2

The concept of Regulated Intramembrane Proteolysis (RIP) evolved from the observation that transmembrane proteins can be cleaved to release the cytosolic fragments that may enter the nucleus to control transcription of other genes [28]. Here we describe the shedding of a type III multipass transmembrane protein, Panx2. As reported for other membrane proteins, Panx2 is cleaved by agents that activate the protein kinase C (PKC) pathway such as in APP, NOTCH and SREBP [29; 30; 31]. Panx2 is a

brain-specific protein whose N-terminal and C-terminal domains are in the cytosol. Using PMA and potent inhibitors (γ-secretase and metalloprotease), we demonstrated that Panx2 is cleaved at the c-terminal fragment (**Figures 4 B-D**). PKC is an intracellular kinase activated by PMA and increases ADAM17 activity [32; 33]. Panx2 acts as a substrate for ADAM17, which in turn triggers intramembrane protease γ-secretase, leading to the cleaving of the Panx2 intracellular domain. Therefore, in response to PKC activation, Panx2 cleavage triggered by ADAM17 at site1 releases a ~25KDa fragment. The second cut mediated by protease γ-secretase releases a smaller fragment, ~17KDa (CTF17). The cleaved Panx2 fragment located in the cytosol was transported to the nucleus (**Figure 4F**).

Organisation and modification of miR9Some in chromatin

Higher-order chromatin organisation is important for gene regulation. Chromatin looping brings remote sequences together in a long-distance genetic switch-on/off process controlled by the locus control region [34]. This phenomenon has been studied for several genes, such as *Igf2* [35], *ß-globin* [36], *Dlx5-Dlx6* [24] and a cytokine gene cluster [37]. Looping spatially connects gene-specific binding sites with promoters and regulatory regions [38]. We analysed the *in vitro* chromatin structure of mNPCs across the 34kb genomic locus that contains miR-9 using a 3C/ChIP loop assay and found a chromatin loop organisation mediated by *Panx2/Polr1c/Mgea5* (**Figure 5**). Active and silent chromatin states can be controlled by specific epigenetic modifications, and chromatin remodelling mediated by accessory proteins, transcriptional factors or chromatin-modifying enzymes [38; 39]. We therefore analysed the histone marks on *Panx2/Polr1c/Mgea5* binding sites on the miR-9 locus and found acetylation (H3Lys9/14ac) to be highly corelated in these sites. This indicates that in the normal state of mNPCs, *Panx2/Polr1c/Mgea5* contributes to transcriptionally active chromatin, forming an 8.4kb loop. Using RNAi, we showed that this loop was mediated by *Panx2* and *Polr1c*. This loop structure was not formed in *Panx2/Polr1c* null mNPCs (**Figures 5 B-C**). *Mgea5* null mNPCs showed 11.2kb loop structure, and it corresponded to the methylated histone mark (**Figure 5D**). We postulated that since *Mgea5* has histone acetyltransferase (HAT) activity [40; 41], its absence would lead to a methylated chromatin state. Thus, *Panx2/Polr1c* mediated an active chromatin-associated loop (8.4kb loop), whereas *Mgea5* mediated a silent chromatin loop (11.2kb loop) formed on the miR-9 locus (**Figures 5 E-F**). Next, we determined how the miR9Some-dependent state of chromatin regulated miR-9 expression. In the wild-type mNPCs, we observed basal level of miR-9 expression. However, in *Panx2/Polr1c/Mgea5* null mNPCs, miR-9 expression levels increased compared to wild-type. Also, a threefold increase in miR-9 levels was observed after miR9Some *knockdown* in mNPCs (**Figures 6 A-D**).

Synergistic role of miR9Some in neuronal differentiation

We also found that miR9Some knockdown upregulated miR-9 three-fold and led to downregulation of *Bace1* (**Figures 6 E-F**). This suggests a regulatory pathway between miR9Some, miR-9 and *Bace1*. Since the miR9Some regulated miR-9 we also questioned if it could modulate neuronal differentiation. We showed that miR9Some knockdown increased neuronal differentiation of mNPCs (**Figures 6 G-I**).

In summary, we identified that miR9Some acts upstream of miR-9 to regulate its expression. Our findings encourage further research to identify more components of the miR9Some to unveil the epigenetic mechanism of miR-9. miR9Some may also have a specific role in the regulation of other miRs, a concept which needs to be explored. Researchers could also identify one or more miRSomes that regulate other miRs' expression. Our work has implications for future therapeutic strategies targeting miR9Some components in miR-9 related NDDs like AD.

Methods

Experimental model and subject details

Ethics Statement

All animal experiments carried out in this study followed the requirements of the Institutional Animal Care and Use Committee at the Monash University (Ethics ID: 22020). All efforts were made to minimize the suffering to the animal.

Cell lines

Neuro-2a Neuroblastoma cells (N2a) are mouse neuroblasts obtained from brain tissue. N2a cells were kindly provided by Zenker Lab. N2a cells were cultured in Dulbecco's Modified Eagle Medium (DMEM) (Cat# 10569010, Gibco) supplemented with 10% fetal bovine serum (Cat#: 10099141,), 100 I.U./mL Penicillin and 100 mg/mL Streptomycin.

HEK293T (Human embryonic kidney) cells were kindly provided by Polo Lab. HEK293T cells were cultured in Dulbecco's Modified Eagle Medium (DMEM) (Cat# 11995065, Gibco) supplemented with 10% fetal bovine serum, 2mM GlutaMAX Supplement (Cat# 35050061, Gibco), 100 I.U./mL Penicillin and 100 mg/mL Streptomycin.

Collaborative Cross mouse model

Collaborative Cross mouse lines (CC) were obtained from Tel Aviv University (TAU), Israel and Geniad, Australia. Brain samples of CC strains were used in this study. We have used 22 CC lines from TAU and 32 lines from Geniad totalling to 54 CC lines. There were 3 CC mice under each strain. CC strains used for this study were between 5-6 weeks and 30-45 weeks. All the mice studied in this project were males. See **Table S1** for the list of CC mice strains used.

Mouse primary neural progenitor cell isolation

Neural progenitor cells (mNPCs) were isolated from hippocampus of the WT C57BL/6 mouse. Briefly, animals were euthanized in a CO2 chamber. The skin around the head region was removed to expose the skull. It was cut open with small scissors without damaging the brain The brain was removed using a spatula and transferred to ice-cold HBSS-Hepes solution. The two hemispheres were separated and the surrounding tissue was cleared until hippocampus was exposed. Hippocampus was carefully detached and stored in 5ml HBSS-Hepes solution. mNPCs were isolated by adding 5ml of Dissociation media to the hippocampus slices. This mixture was incubated at 37^{o}C for 15 min. Next, the tissue was triturated 10 times with a 5mL plastic pipette to dislodge the pellet and was incubated again for 15 min at 37°C. Then 1 volume of ice-cold Solution 3 was added to inactivate the Trypsin and mixed gently by pipetting up and down using a 10mL plastic pipette. The cells were passed through a 70 µm strainer into a 50 mL falcon tube and centrifuged for 5 min at 1300 rpm at 4°C. The supernatant was removed, and the cells were resuspended in 10 mL ice cold Solution 2. They were centrifuged for 10 min at 2000 rpm at 4°C and resuspended in 2 mL ice cold Solution 3. The centrifugation was repeated for 7 min at 1500 rpm at 4°C. The cells were finally resuspended in 1 mL NPC growth medium.

Mouse NPC culture

mNPCs were maintained on tissue culture-treated polystyrene plates with cell culture qualified Poly-L ornithine (PLO) (Cat# P4957, Sigma)/ Laminin (Cat# L2020, Sigma) solution in DMEM (Cat# 10565018, Gibco). The mNPCs were split every 3 – 4 days using Accutase (Cat# 07920, Stem Cell Technologies).

Hippocampus dissection of CC brain

Frozen brain samples were removed using a long micro spatula to a petri dish containing RNAlater-ICE solution to protect the tissue from RNase. The brain was transferred to a wet filter paper and cut using a razor blade through the middle of the tissue. Hippocampus was dissected gently using two short spatulas. In brief, the spatula tips were positioned near the junction between the cortex and cerebellum,

the cortical hemisphere was peeled off to expose the hippocampus. Carefully the extra white matter surrounding the hippocampus was removed. Holding the brain with one tip and placing the other tip just under the caudal side, hippocampus was rolled off from the remaining tissue.

Plasmid mutagenesis

The Panx2 c-terminal fragment (CTF) plasmid in pcDNA3.1 backbone was purchased from Vector builder. We used QuikChange II XL Site Directed Mutagenesis kit (Cat#: 200523, Agilent Technologies) according to the manufacturer's protocol. Briefly, we searched the database (NLSdb, cNLS mapper) to locate the nuclear localisation signal (NLS) of Panx2. Then primers were designed to generate deletion mutation of NLS sequence (△341-343) in the Panx2 CTF. PCR was performed using PfuUltra High-Fidelity DNA polymerase. The PCR products were purified and digested using DpnI. We performed transformation using XL1-Blue electroporation-competent cells. The clones were picked and verified by sequencing. Oligonucleotides used in this method is listed in **Table S2**.

Immunocytochemistry

Cells were treated in different experimental conditions for specified time. Then, the cells were fixed in 4% paraformaldehyde (Cat#: Sc-281692, Santa Cruz Biotechnology) for 10min at room temperature. The plates were briefly rinsed in PBS and permeabilised for 30min at room temperature using permeabilization buffer (PBS-0.1% Tween20, 5% goat serum). The cells were incubated with specific primary antibodies (Panx2, Polr1c, Mgea5, ß III Tubulin) at 4^{o}C overnight. The following day cells were washed with PBS for 10min/3washes. We added secondary antibody (Alexa Fluor 546 anti-Rabbit) to the cells and incubated for 1hr at room temperature in dark setup. We repeated the washing step with PBS for 10min/3washes protected from light. The cells were counterstained by DAPI for 5min at room temperature in dark and imaged using confocal SP5 5 channel microscope.

ChIP-seq assay, library preparation, and sequencing

ChIP-seq was performed as described previously in [42] with slight modifications. Briefly, mNPCs were trypsinized and washed once in PBS. Cells were resuspended in PBS and crosslinked in 1% formaldehyde solution (Cat# 252549, Sigma) for 8 min at room temperature. Then glycine was added at a final concentration of 0.125M to quench the reaction for 5 min. Cells were washed twice in PBS and suspended in SDS-ChIP buffer (20mM Tris-HCl, pH 8, 150mM NaCl, 2mM EDTA, 0.1% SDS, 1% Triton X-100 and protease inhibitor (Cat# C12010011, Diagenode)). Then, chromatin was sheared using a Diagenode Bioruptor Plus with high power mode for 40 cycles (sonication cycle: 30 sec ON, 30 sec OFF) until DNA was fragmented to 200–700bp. Sonicated chromatin was centrifuged at 4^{o}C for 10 min and

pre-cleared using Dynabeads Protein A/G beads for 1hr at 4^{o}C with end-to-end rotation. Cleared supernatant was incubated with gene-specific primary antibody (Panx2, Polr1c, Mgea5) at 4^{o}C overnight with end-to-end rotation. Protein A/G beads were added to the overnight incubated antibody-protein complex for 2 hrs at 4^{o}C with end-to-end rotation to immunoprecipitate the chromatin. This complex was washed six times (5 min/wash at 4^{o}C with rotation) in Low-salt buffer (twice, 50 mM HEPES pH 7.5, 150mM NaCl, 1mM EDTA, 1% Triton X-100, 0.1% sodium deoxycholate), High-salt buffer (once, 50 mM HEPES pH 7.5, 500mM NaCl, 1mM EDTA, 1% Triton X-100, 0.1% sodium deoxycholate), LiCl wash buffer (once, 10mMTris-HCl pH 8.0, 1mM EDTA, 0.5% sodium deoxycholate, 0.5% NP-40, 250mM LiCl) and TE buffer (twice, 10mMTris-HCl pH 8.0, 1mM EDTA pH 8). The chromatin was eluted and reverse-crosslinked in SDS-Elution buffer (1% SDS, 50mMTris-HCl pH 8.0, 10mM EDTA pH 8) at 65^{o}C overnight. ChIP DNA was treated with 1µl RNase (10mg/ml) for 1hr and 3µl Proteinase K (20mg/ml) for 3hrs at 37^{o}C. The purified ChIP DNA and Input DNA (reserved before adding antibody but reverse crosslinked and purified) was used to prepare ChIP-seq libraries using NEBNext Ultra II DNA Library Prep Kit for Illumina (Cat. E7645S, New England Biolabs) DNA samples were ligated to adaptor oligos for multiplex sequencing (Cat. E7335G, New England Biolabs). ChIP-seq was performed using Illumina Hiseq3000/4000 sequencing platform.

3C and ChiP loop assay

We performed 3C and ChiP loop assay as described in [24] with slight modifications. Briefly, mNPCs were crosslinked for 10min at room temperature with continuous mixing. This reaction was quenched by glycine at a final concentration of 0.125M for 5min on ice. The cells were washed in PBS once. Then, the pellet was suspended in nuclear lysis buffer (10mM Tris, pH 8, 10mM NaCl, 0.2% NP-40 and protease inhibitor) and incubated on ice for 15min. The isolated chromatin was treated with 20% SDS for 1hr at 37^{o}C with mixing at 1000rpm. Next, 20% Triton X-100 was added and incubated for 1hr at 37^{o}C with mixing at 1000rpm. The restriction digestion was performed with restriction enzyme ApaLI (Cat#: R0507M, NEB) overnight at 37^{o}C for 16hrs. We pre-cleared the digested chromatin with Protein A/G beads for 1hr at 4^{o}C with end-to-end rotation. We incubated the pre-cleared chromatin with antibodies to Panx2, Polr1c, Mgea5, dimethylated H3-Lys9, acetylated H3-Lys9/Lys14 and nonimmune rabbit serum at 4^{o}C for 6hrs with rotation. Then incubated the chromatin-antibody complex with Protein A/G beads overnight at 4^{o}C with rotation. We washed the complex following the protocol described above. The beads were suspended in 50µl of ligation buffer and incubated at 16^{o}C overnight with T4 DNA ligase for ligation. This mixture was eluted with vigorous shaking at 1000rpm, 65^{o}C for 1hr. Then, treated sequentially with RNase A at 37^{o}C for 30min and Proteinase K at 68^{o}C for 6hrs for reverse crosslinking. We purified the samples using phenol/chloroform extraction. The ligated DNA was amplified using Kapa fast Sybr green Master mix in LC480 using the manufacturer's recommendations. For 3C assay, we performed similar steps excluding the immunoprecipitation step. We designed unidirectional primers for stringent PCR amplifications. The PCR amplifications occurred reproducibly due to the short distance. As an internal

control, we designed another primer set C1 and C2 which fell completely out of the digested fragment region in the miR-9 locus. We also used ß-actin specific primers A1 and A2 for validation. We also confirmed that all the primer combinations could be amplified by using a ApaLI digested BAC clone (RP23-207N5, BACPAC genomics) containing the fragmented 34kb miR-9 locus. We tested the primer combinations in genomic DNA and nonimmune rabbit serum to confirm the absence of nonspecific reactions following the similar protocol. Oligonucleotides used in this method is listed in **Table S2**.

Lentiviral transduction

All the lentivirus particles were purchased from Vector builder. We produced the second-generation lentivirus by transient transfection of HEK293T cells with lentiviral particles (Panx2, Polr1c, Mgea5 and miR-9), pPax2 (packaging plasmid) and pMD2.G (envelope plasmid) in Optimem (Cat#: 31985070, Thermo Fisher Scientific) using Lipofectamine LTX reagent (Cat#: 15338100, Thermo Fisher Scientific). The complex was harvested after 72hrs, filtered through 0.45µm Durapore Membrane Filter (Cat#: S2HVU01RE, Merck Millipore) and concentrated using Amicon Ultra-15 Centrifugal Filter Units (Cat#: UFC910096, Merck Millipore). The mNPCs were infected using the lentiviruses and stable plasmid expression was generated using Puromycin selection.

Co-IP

Co-immunoprecipitation was performed using Dynabeads Co-Immunoprecipitation Kit (Cat#: 14321D, Life Technologies) following the manufacturer's protocol. Before preparing the cells for co-IP, we coupled 5ug of antibody (Panx2, Polr1c, Mgea5 and Rb igg) to the epoxy beads overnight at 4^{o}C. Beads were washed as per the kit's instruction. mNPCs were grown overnight at 37^{o}C. The cells were lysed in detergent lysis buffer and washed once in PBS. The cell lysate was coupled to the antibody-bead complex and incubated at 4^{o}C on a roller for 30min. This mixture was washed and eluted. The purified protein was subjected to immunoblotting.

Live cell imaging

For the live antibody uptake assay and live cell imaging, antibody directed against Panx2 CTF were fluorescently labelled using Alexa Fluor 546 anti-Rabbit secondary antibody [43]. In short, mNPCs were cultured at 37^{o}C overnight in a fluoro dish (collected from MMI facility, Monash University). Next day, 1µg of Panx2 antibody was mixed with 2µg of Alexa Fluor 546 such that the total volume was adjusted to 25µl. This mixture was incubated for 15min at room temperature. 12.5µl of this mixture was added to 87.5µl of the growth medium to a 50-fold dilution. The cells were incubated with this mixture for 30min at

4^{o}C. Then, the cells were treated with DMSO (control) and PMA (treatment) for 2hrs at 37^{o}C. For live antibody uptake assay, cells were fixed immediately, counterstained by DAPI and imaged using 3i Marianas. For live cell imaging, we used 3iMarianas to create a movie to observe antibody internalisation. This process was captured for 2hrs and analysed using Image J plugin slide-book. We also performed another experiment in which the primary antibody was completely omitted from the mixture to control for the specificity of the experiment.

Shedding assay

Shedding assay was performed as described in [44] with few modifications. mNPCs were grown overnight at 37^{o}C in pre-coated six well plates for the assay. Next day, Phorbol 12-myristate 13-acetate (PMA Cat#: P1585, Sigma) was diluted in Optimem and added to the cells. The treated cells were incubated at 37^{o}C for 2hrs. For inhibition assay, we treated the overnight grown culture with 1µM DAPT (Cat#: D5942, Sigma) and 50 µM GM6001 (Cat#: M5939, Sigma) for 20hrs. Then, PMA was added at specific timepoint for 2hrs. The cells were lysed in RIPA buffer (Cat#: 89900, Thermo Fisher Scientific) and rotated at 4^{o}C for 30min. The samples were boiled for 5min. Immunoblotting was performed using Panx2 antibodies. ß-actin was used as loading control.

Nuclear enriched lysis, immunoprecipitation, and immunoblotting

For nuclear isolation, mNPCs were treated with PMA and vehicle (DMSO) at 37^{o}C for 2hrs followed by nuclei isolation using NE-PER Nuclear and Cytoplasmic Extraction Reagents kit (Cat#: 78833, Thermo Fisher Scientific) following the manufacturers protocol.

For Immunoprecipitation (IP), the nuclear extract was pre-cleared with Protein A/G beads for 1hr at 4^{o}C with end-to-end rotation. Next, c-terminal specific Panx2 antibody was added to the lysate and incubated overnight at 4^{o}C with end-to-end rotation. The immunocomplex were captured by adding Protein A/G beads for 2hrs at 4^{o}C with end-to-end rotation. The beads were washed in IP wash buffer (5M NaCl and 1M Tris, pH8) three times/5min at 4^{o}C with end-to-end rotation. Then the beads were eluted in 2XT sample loading buffer (Cat#: 1610791, Biorad). The beads were boiled for 10min at 95^{o}C at 1000rpm to completely dissociate the beads from the immunocomplex and subjected to immunoblotting.

For immunoblotting (western blotting), protein samples were subjected to SDS-PAGE. The samples were mixed with 2x Laemmli buffer (Cat#: 1610737, Bio-rad) and boiled for 5min at 95^{o}C. It was resolved on 4–20% Mini-PROTEAN TGX Precast Protein Gel (Cat#: 4561093, Bio-rad). The protein gels were transferred using the iBlot2 mini gel Transfer Stack system (Cat#: IB24002, Thermo Fisher Scientific) and iBlot2 gel transfer device (Cat#: IB21001, Thermo Fisher Scientific) for 7 min at 25V. Membranes were blocked with 3% BSA in TBS-0.1%Tween 20 for 1hr at room temperature. The primary antibodies (Panx2,

Polr1c, Mgea5, B-actin) were added to the membrane and incubated overnight at 4^{o}C with continuous agitation. The membranes were washed in TBST for 3 times with 10min mixing between each washes. An HRP-conjugated secondary antibody (Anti-Rabbit IgG–Peroxidase) was added to the membrane for 1hr at room temperature. 10 min wash was repeated for 3 times with constant agitation. We detected the bands using SuperSignal West Atto (Cat#: A38554, Thermo Fisher Scientific).

RNA extraction and real-time PCR analysis

RNA was isolated using miR Vana miRNA isolation kit following the manufacturer's protocol. Briefly, cells were grown in different experimental conditions and harvested using 0.05% Trypsin-edta. Cells were washed in PBS and pellet lysed in lysis buffer provided with the kit. For miR isolation, miR enrichment homogenate solution was added. For cDNA synthesis, iScript cDNA synthesis kit was used. For Taqman assays, we used Taqman advanced miRNA cDNA synthesis kit. The PCR reaction was performed in Roche LC480 (Roche) using Kapa fast Sybr green Master mix for mRNA and Taqman Fast Advance master mix for miR. The gene expression data was normalised to Gapdh (mRNA) and mmu-mir-16/mmu-mir-191 (miR).

ChIP-seq analysis

For ChIP-seq data analysis, raw data was trimmed down using program trim galore to remove adapter sequences. We also used –paired function in this program to validate paired end reads and removed all the low-quality sequence-reads. We assessed the quality of sequencing data using FastQC. Mm10 was used as reference genome and alignment was performed using Bowtie v2.3.5. MACS3 software was used for peak calling to evaluate the significance of enriched binding regions and the spatial resolution of binding sites against the input control. We used –pvalue with a cut-off $p<0.01$ for the analysis. When an empirical cut-off value is specified, MACS3 calculated the fold enrichment of a peak in the treatment file above the input file. It also generates a coverage map along the genome and provides information related to chromosome name, peak location and fold enrichment. All ChIP-seq data from two or more experiments were analysed independently. We have used Integrated genome Viewer (IGV) to view the enriched peak against the mouse genome as reference sequence.

siRNA transfection on mNPCs

For siRNA knockdown experiments, mNPCs were detached from the cell culture plates using Accutase. Then, centrifuged at 200rpm for 5min at room temperature, supernatant was removed, and pellet dissolved in complete growth medium. Cells were then distributed into pre-coated 24 well plates to perform knockdown. Transfection was performed directly before the cells attach to the surface of the plate using lipofectamine RNAimax (Cat. 13778075, Invitrogen) following the manufacturer's protocol for

48hrs. For few of the genes, we performed forward transfection wherein the cells were allowed to grow overnight and then transfected the next day in a similar manner to increase the efficiency of transfection. For mNPC differentiation experiments, we grew cells and transfected them for 48hrs. Then re-transfected the cells again and differentiated them for three days. We targeted for knockdown efficiency above 70% for all the siRNAs used in this study.

Pathway enrichment analysis for candidate gene prioritisation

Functional enrichment analysis for Gene Ontology (GO) terms was performed using Bioinformatics Platform DAVID, EBI and Kegg Pathway analysis using *Mus musculus* as background. Modules enriched in neurogenesis, neurodegenerative disorders and transcription related functions within the GO: Biological Process, GO: Molecular Process and Disease section were extracted.

QTL analysis

The framework for QTL analysis was implemented using R. HAPPY package is available as an R package called happy.hbrem. To run happy in R, we also installed g.data and multicore.

We downloaded the condensed genome library from:

http://mtweb.cs.ucl.ac.uk/mus/www/preCC/CC-2018/LIFTOVER/

happy.preCC.R script was obtained from

http://mtweb.cs.ucl.ac.uk/mus/www/preCC/R.CD/happy.preCC.R which was used to set the environment for mapping in R. miR expression profiling data was used to create phenotypic file. Then, condensed genome library was loaded which scanned for the phenotypic files to create an association between the trait in question and genetic markers at a particular genomic locus. Genome wide significance for miR trait were computed at 50% and 95% threshold. We also used Gene miner software to perform the QTL analysis.

Luciferase assay

mNPCs were plated in 24 well PLO-Laminin coated cell culture plates for luciferase assay. mNPCs were co-transfected with siRNAs for Panx2, Polr1c and Mgea5 and miR-9 promoter expressing lentiviral particles in different combinations. A mutant miR-9 promoter expressing lentiviral particles were also used. A scrambled lentiviral negative control was used to measure the background reporter activity. Cells were lysed 48hrs after transfection. Dual Luciferase Assay System (Cat#: E1910, Promega) was used to

measure the luciferase activity according to the manufacturer's instructions. The Firefly luciferase activity was analysed relative to the Renilla luciferase activity in the same sample by using a multi-mode microplate reader (FLUOstar Omega, BMG Labtek).

Quantification and statistical analysis

We used GraphPad Prism software to perform the quantitative analysis for all the experimental conditions. For comparison between two datasets, we used Unpaired T-test. To test between multiple experimental variables, we performed One-way Anova. All the p-values permuted to $p<0.05$ were considered significant. The level of significance in all the measurements were represented as $* \ p < 0.05$, $** \ p < 0.005$, $*** \ p < 0.0005$, $**** \ p < 0.0001$. Statistical parameters specifying the total number of measurements (n), standard error for precision (mean ± SEM) and p-values were reported in the individual figure legends.

Declarations

Data and Code Availability

The ChIP sequencing data that support the findings of this study are openly available in Gene Expression Omnibus (GEO), reference number: GSE202645.

Deposited Data

Raw data from Figures 2, 3, 4 and 5, Figures S2, S4 and S5 were deposited on Mendeley at (doi:10.17632/9ms65tkv9r.1). Link to preview data:

https://data.mendeley.com/datasets/9ms65tkv9r/draft?a=cdf053aa-94f8-4536-9262-bb4942813860

Any additional information required to re-analyse the data reported in this paper is available from the lead contact upon request.

Acknowledgments

We acknowledge Dr Zhiyong He for the helpful discussions. We are very grateful to Drs Pratibha Tripathi and Partha Das for valuable suggestions on ChIP-seq. We also express our gratitude to Ms Xin-ran Chen.

We thank Dr Ilona Binenbaum for the training on QTL analysis. This work was supported by the program of “Genetic diversity in the collaborative cross model recapitulates miRNA mediated neurogenesis” (ID: 281589068), which was a donation of Apex Biotech Research Pty Ltd to Monash University. D.K. is funded by a PhD scholarship from Monash University (CF-MGS and FITS).

Author contributions

Conceptualization, Z.C.X. and D.K.; Methodology, D.K. and Z.C.X.; Validation, Z.C.X. and D.K.; Formal Analysis, D.K., F.A.I., G.M. and Z.C.X.; Investigation, D.K. and Z.C.X.; Resources, F.A.I., G.M., D.K. and Z.C.X.; Writing – Original Draft, D.K.; Writing – Review & Editing, D.K. Z.C.X, F.A.I. and G.M.; Funding Acquisition, Z.C.X.; Supervision, Z.C.X.

Declaration of interests

The authors declare no competing interests.

References

1 LIU, W.; WANG, X. Prediction of functional microRNA targets by integrative modeling of microRNA binding and target expression data. **Genome Biol,** v. 20, n. 1, p. 18, 01 22 2019. ISSN 1474-760X. Disponível em: < https://www.ncbi.nlm.nih.gov/pubmed/30670076 >.

2 PIRCS, K.; PETRI, R.; JAKOBSSON, J. Crosstalk between MicroRNAs and Autophagy in Adult Neurogenesis: Implications for Neurodegenerative Disorders. **Brain Plast,** v. 3, n. 2, p. 195-203, Aug 10 2018. ISSN 2213-6312. Disponível em: < https://www.ncbi.nlm.nih.gov/pubmed/30151343 >.

3 HARROW, J. et al. GENCODE: producing a reference annotation for ENCODE. **Genome Biol,** v. 7 Suppl 1, p. S4.1-9, 2006. ISSN 1474-760X. Disponível em: < https://www.ncbi.nlm.nih.gov/pubmed/16925838 >.

4 COOLEN, M.; KATZ, S.; BALLY-CUIF, L. miR-9: a versatile regulator of neurogenesis. **Front Cell Neurosci,** v. 7, p. 220, Nov 2013. ISSN 1662-5102. Disponível em:

< https://www.ncbi.nlm.nih.gov/pubmed/24312010 >.

5 EBERT, M. S.; SHARP, P. A. Roles for microRNAs in conferring robustness to biological processes. **Cell,** v. 149, n. 3, p. 515-24, Apr 27 2012. ISSN 1097-4172. Disponível em: < https://www.ncbi.nlm.nih.gov/pubmed/22541426 >.

6 ZHAO, C. et al. A feedback regulatory loop involving microRNA-9 and nuclear receptor TLX in neural stem cell fate determination. **Nat Struct Mol Biol,** v. 16, n. 4, p. 365-71, Apr 2009. ISSN 1545-9985. Disponível em: < https://www.ncbi.nlm.nih.gov/pubmed/19330006 >.

7 WANG, Z. et al. miR-9-5p modulates the progression of Parkinson's disease by targeting SIRT1. **Neurosci Lett,** v. 701, p. 226-233, 05 14 2019. ISSN 1872-7972. Disponível em: < https://www.ncbi.nlm.nih.gov/pubmed/30826419 >.

8 HÉBERT, S. S. et al. Loss of microRNA cluster miR-29a/b-1 in sporadic Alzheimer's disease correlates with increased BACE1/beta-secretase expression. **Proc Natl Acad Sci U S A,** v. 105, n. 17, p. 6415-20, Apr 2008. ISSN 1091-6490. Disponível em: < https://www.ncbi.nlm.nih.gov/pubmed/18434550 >.

9 BUCKLEY, N. J. et al. The role of REST in transcriptional and epigenetic dysregulation in Huntington's disease. **Neurobiol Dis,** v. 39, n. 1, p. 28-39, Jul 2010. ISSN 1095-953X. Disponível em: < https://www.ncbi.nlm.nih.gov/pubmed/20170730 >.

10 HARAMATI, S. et al. miRNA malfunction causes spinal motor neuron disease. **Proc Natl Acad Sci U S A,** v. 107, n. 29, p. 13111-6, Jul 2010. ISSN 1091-6490. Disponível em: < https://www.ncbi.nlm.nih.gov/pubmed/20616011 >.

11 BARBANO, R. et al. Stepwise analysis of MIR9 loci identifies miR-9-5p to be involved in Oestrogen regulated pathways in breast cancer patients. **Sci Rep,** v. 7, p. 45283, 03 27 2017. ISSN 2045-2322. Disponível em: < https://www.ncbi.nlm.nih.gov/pubmed/28345661 >.

12 CHURCHILL, G. A. et al. The Collaborative Cross, a community resource for the genetic analysis of complex traits. **Nat Genet,** v. 36, n. 11, p. 1133-7, Nov 2004. ISSN 1061-4036. Disponível em: < https://www.ncbi.nlm.nih.gov/pubmed/15514660 >.

13 RAM, R.; MORAHAN, G. Complex Trait Analyses of the Collaborative Cross: Tools and Databases. **Methods Mol Biol,** v. 1488, p. 121-129, 2017. ISSN 1940-6029. Disponível em: < https://www.ncbi.nlm.nih.gov/pubmed/27933522 >.

14 XIE, H. et al. MiR-9 Regulates the Expression of BACE1 in Dementia Induced by Chronic Brain Hypoperfusion in Rats. **Cell Physiol Biochem,** v. 42, n. 3, p. 1213-1226, 2017. ISSN 1421-9778. Disponível em: < https://www.ncbi.nlm.nih.gov/pubmed/28683457 >.

15 WANG, W. X. et al. The expression of microRNA miR-107 decreases early in Alzheimer's disease and may accelerate disease progression through regulation of beta-site amyloid precursor protein-cleaving enzyme 1. **J Neurosci,** v. 28, n. 5, p. 1213-23, Jan 2008. ISSN 1529-2401. Disponível em: < https://www.ncbi.nlm.nih.gov/pubmed/18234899 >.

16 ROSHAN, R. et al. Regulation of BACE1 by miR-29a/b in a cellular model of Spinocerebellar Ataxia 17. **RNA Biol,** v. 9, n. 6, p. 891-9, Jun 2012. ISSN 1555-8584. Disponível em: < https://www.ncbi.nlm.nih.gov/pubmed/22664922 >.

17 THORVALDSDÓTTIR, H.; ROBINSON, J. T.; MESIROV, J. P. Integrative Genomics Viewer (IGV): high-performance genomics data visualization and exploration. **Brief Bioinform,** v. 14, n. 2, p. 178-92, Mar 2013. ISSN 1477-4054. Disponível em: < https://www.ncbi.nlm.nih.gov/pubmed/22517427 >.

18 JENUWEIN, T.; ALLIS, C. D. Translating the histone code. **Science,** v. 293, n. 5532, p. 1074-80, Aug 10 2001. ISSN 0036-8075. Disponível em: < https://www.ncbi.nlm.nih.gov/pubmed/11498575 >.

19 YOSHIDA, K.; ASAOKA, Y.; NISHIZUKA, Y. Platelet activation by simultaneous actions of diacylglycerol and unsaturated fatty acids. **Proc Natl Acad Sci U S A,** v. 89, n. 14, p. 6443-6, Jul 15 1992. ISSN 0027-8424. Disponível em: < https://www.ncbi.nlm.nih.gov/pubmed/1631141 >.

20 ARRIBAS, J. et al. Diverse cell surface protein ectodomains are shed by a system sensitive to metalloprotease inhibitors. **J Biol Chem,** v. 271, n. 19, p. 11376-82, May 10 1996. ISSN 0021-9258. Disponível em: < https://www.ncbi.nlm.nih.gov/pubmed/8626692 >.

21 AMIT, T. et al. Shedding of growth hormone-binding protein is inhibited by hydroxamic acid-based protease inhibitors: proposed mechanism of activation of growth hormone-binding protein secretase. **J Endocrinol,** v. 169, n. 2, p. 397-407, May 2001. ISSN 0022-0795. Disponível em: < https://www.ncbi.nlm.nih.gov/pubmed/11312156 >.

22 HUSSAIN, I. et al. Characterization of the ectodomain shedding of the beta-site amyloid precursor protein-cleaving enzyme 1 (BACE1). **J Biol Chem,** v. 278, n. 38, p. 36264-8, Sep 19 2003. ISSN 0021-9258. Disponível em: < https://www.ncbi.nlm.nih.gov/pubmed/12857759 >.

23 PARVATHY, S. et al. Alzheimer's amyloid precursor protein alpha-secretase is inhibited by hydroxamic acid-based zinc metalloprotease inhibitors: similarities to the angiotensin converting enzyme secretase. **Biochemistry,** v. 37, n. 6, p. 1680-5, Feb 10 1998. ISSN 0006-2960. Disponível em: < https://www.ncbi.nlm.nih.gov/pubmed/9484239 >.

24 HORIKE, S. et al. Loss of silent-chromatin looping and impaired imprinting of DLX5 in Rett syndrome. **Nat Genet,** v. 37, n. 1, p. 31-40, Jan 2005. ISSN 1061-4036. Disponível em: < https://www.ncbi.nlm.nih.gov/pubmed/15608638 >.

25 ONOS, K. D. et al. Toward more predictive genetic mouse models of Alzheimer's disease. **Brain Res Bull,** v. 122, p. 1-11, Apr 2016. ISSN 1873-2747. Disponível em: < https://www.ncbi.nlm.nih.gov/pubmed/26708939 >.

[26] MOLENHUIS, R. T. et al. Modeling the quantitative nature of neurodevelopmental disorders using Collaborative Cross mice. **Mol Autism,** v. 9, p. 63, 2018. ISSN 2040-2392. Disponível em: < https://www.ncbi.nlm.nih.gov/pubmed/30559955 >.

[27] RISTORI, E. et al. A Dicer-miR-107 Interaction Regulates Biogenesis of Specific miRNAs Crucial for Neurogenesis. **Dev Cell,** v. 32, n. 5, p. 546-60, Mar 2015. ISSN 1878-1551. Disponível em: < https://www.ncbi.nlm.nih.gov/pubmed/25662174 >.

[28] BROWN, M. S. et al. Regulated intramembrane proteolysis: a control mechanism conserved from bacteria to humans. **Cell,** v. 100, n. 4, p. 391-8, Feb 18 2000. ISSN 0092-8674. Disponível em: < https://www.ncbi.nlm.nih.gov/pubmed/10693756 >.

[29] VASSAR, R. et al. Beta-secretase cleavage of Alzheimer's amyloid precursor protein by the transmembrane aspartic protease BACE. **Science,** v. 286, n. 5440, p. 735-41, Oct 22 1999. ISSN 0036-8075. Disponível em: < https://www.ncbi.nlm.nih.gov/pubmed/10531052 >.

[30] BROU, C. et al. A novel proteolytic cleavage involved in Notch signaling: the role of the disintegrin-metalloprotease TACE. **Mol Cell,** v. 5, n. 2, p. 207-16, Feb 2000. ISSN 1097-2765. Disponível em: < https://www.ncbi.nlm.nih.gov/pubmed/10882063 >.

[31] DUNCAN, E. A. et al. Second-site cleavage in sterol regulatory element-binding protein occurs at transmembrane junction as determined by cysteine panning. **J Biol Chem,** v. 273, n. 28, p. 17801-9, Jul 10 1998. ISSN 0021-9258. Disponível em: < https://www.ncbi.nlm.nih.gov/pubmed/9651382 >.

[32] MÜLLBERG, J. et al. The soluble interleukin-6 receptor is generated by shedding. **Eur J Immunol,** v. 23, n. 2, p. 473-80, Feb 1993. ISSN 0014-2980. Disponível em: < https://www.ncbi.nlm.nih.gov/pubmed/8436181 >.

[33] _____. Protein kinase C activity is rate limiting for shedding of the interleukin-6 receptor. **Biochem Biophys Res Commun,** v. 189, n. 2, p. 794-800, Dec 15 1992. ISSN 0006-291X. Disponível em:

< https://www.ncbi.nlm.nih.gov/pubmed/1335247 >.

34 BULGER, M.; GROUDINE, M. Looping versus linking: toward a model for long-distance gene activation. **Genes Dev,** v. 13, n. 19, p. 2465-77, Oct 01 1999. ISSN 0890-9369. Disponível em: < https://www.ncbi.nlm.nih.gov/pubmed/10521391 >.

35 MURRELL, A.; HEESON, S.; REIK, W. Interaction between differentially methylated regions partitions the imprinted genes Igf2 and H19 into parent-specific chromatin loops. **Nat Genet,** v. 36, n. 8, p. 889-93, Aug 2004. ISSN 1061-4036. Disponível em: < https://www.ncbi.nlm.nih.gov/pubmed/15273689 >.

36 TOLHUIS, B. et al. Looping and interaction between hypersensitive sites in the active beta-globin locus. **Mol Cell,** v. 10, n. 6, p. 1453-65, Dec 2002. ISSN 1097-2765. Disponível em: < https://www.ncbi.nlm.nih.gov/pubmed/12504019 >.

37 SPILIANAKIS, C. G.; FLAVELL, R. A. Long-range intrachromosomal interactions in the T helper type 2 cytokine locus. **Nat Immunol,** v. 5, n. 10, p. 1017-27, Oct 2004. ISSN 1529-2908. Disponível em: < https://www.ncbi.nlm.nih.gov/pubmed/15378057 >.

38 CAI, S.; LEE, C. C.; KOHWI-SHIGEMATSU, T. SATB1 packages densely looped, transcriptionally active chromatin for coordinated expression of cytokine genes. **Nat Genet,** v. 38, n. 11, p. 1278-88, Nov 2006. ISSN 1061-4036. Disponível em: < https://www.ncbi.nlm.nih.gov/pubmed/17057718 >.

39 WILSON, C. B. et al. DNA methylation and the expanding epigenetics of T cell lineage commitment. **Semin Immunol,** v. 17, n. 2, p. 105-19, Apr 2005. ISSN 1044-5323. Disponível em: < https://www.ncbi.nlm.nih.gov/pubmed/15737572 >.

40 TOLEMAN, C. et al. Characterization of the histone acetyltransferase (HAT) domain of a bifunctional protein with activable O-GlcNAcase and HAT activities. **J Biol Chem,** v. 279, n. 51, p. 53665-73, Dec 2004. ISSN 0021-9258. Disponível em: < https://www.ncbi.nlm.nih.gov/pubmed/15485860 >.

41 HAYAKAWA, K. et al. Epigenetic switching by the metabolism-sensing factors in the generation of orexin neurons from mouse embryonic stem cells. **J Biol Chem,** v. 288, n. 24, p. 17099-110, Jun 14 2013. ISSN 1083-351X. Disponível em: < https://www.ncbi.nlm.nih.gov/pubmed/23625921 >.

42 BRIND'AMOUR, J. et al. An ultra-low-input native ChIP-seq protocol for genome-wide profiling of rare cell populations. **Nat Commun,** v. 6, p. 6033, Jan 21 2015. ISSN 2041-1723. Disponível em: < https://www.ncbi.nlm.nih.gov/pubmed/25607992 >.

43 COUMAILLEAU, F. et al. Directional Delta and Notch trafficking in Sara endosomes during asymmetric cell division. **Nature,** v. 458, n. 7241, p. 1051-5, Apr 23 2009. ISSN 1476-4687. Disponível em: < https://www.ncbi.nlm.nih.gov/pubmed/19295516 >.

44 SAHIN, U. et al. A sensitive method to monitor ectodomain shedding of ligands of the epidermal growth factor receptor. **Methods Mol Biol,** v. 327, p. 99-113, 2006. ISSN 1064-3745. Disponível em: < https://www.ncbi.nlm.nih.gov/pubmed/16780215 >.

Supplementary Information

Tables S1-S5 are not available with this version.

Figures

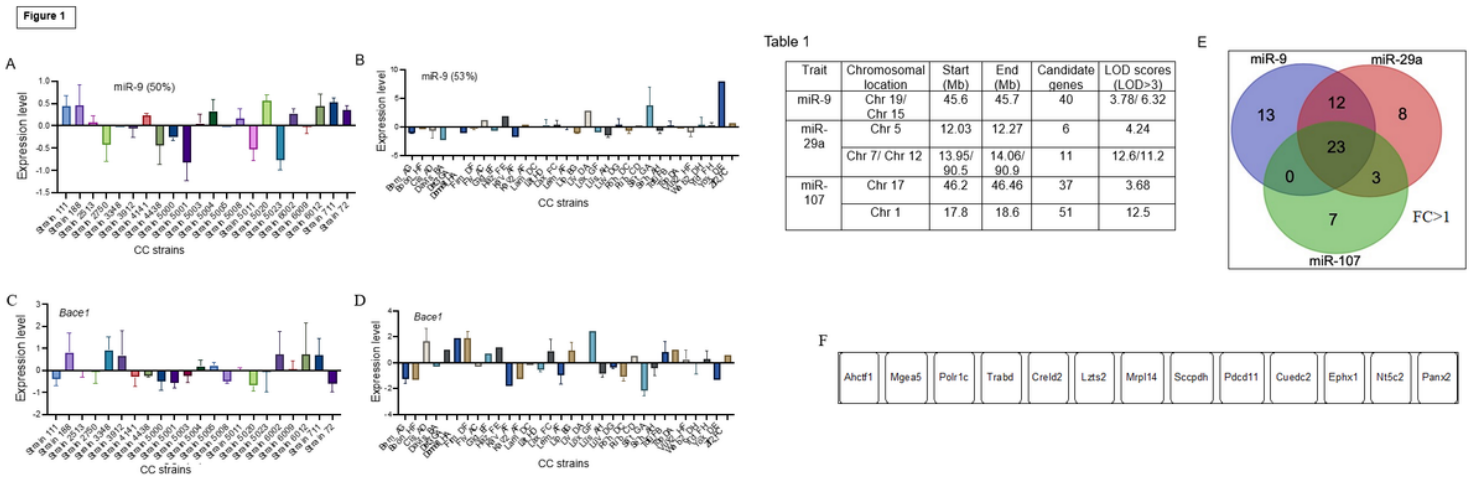

Figure 1

miR expression profiling in CC strains and QTL mapping to identify upstream candidates.

(A) Expression of miR-9 in hippocampi of 5-6 week old CC mice.

(B) Expression of miR-9 in hippocampi of 30-40 week old CC mice.

(C) Expression of *Bace1* in hippocampi of 5-6 week old CC mice.

(D) Expression of *Bace1* in hippocampi of 30-40 week old CC mice.

The percentage of CC mice showing the inverse correlation of miRs to *Bace1* expression- (A) miR-9-50% and (B) miR-9 53%. Data from three CC mice hippocampi/strain for all age-groups represented as mean ± SEM.

(Table 1) Mapping of QTLs associated with miR-9/29a/107 expression in CC lines. 131 candidate genes were identified in the QTL regions by reference to current genome assembly.

(E) Venn Diagram depicting the overlap of genes with fold change (FC) > 1 in miR-9/29a/107 expression performed using RNAi and qPCR. 23 candidates were shortlisted (out of 131) for Bioinformatics analysis. Data from three individual experiments are shown here.

(F) Candidate gene prioritisation revealed 13 candidates- *Ahctf1*, *Mgea5*, *Polr1c*, *Trabd*, *Creld2*, *Lzts2*, *Mrpl14*, *Sccpdh*, *Pdcd11*, *Cuedc2*, *Ephx1*, *Nt5C2* and *Panx2* that were selected for further study.

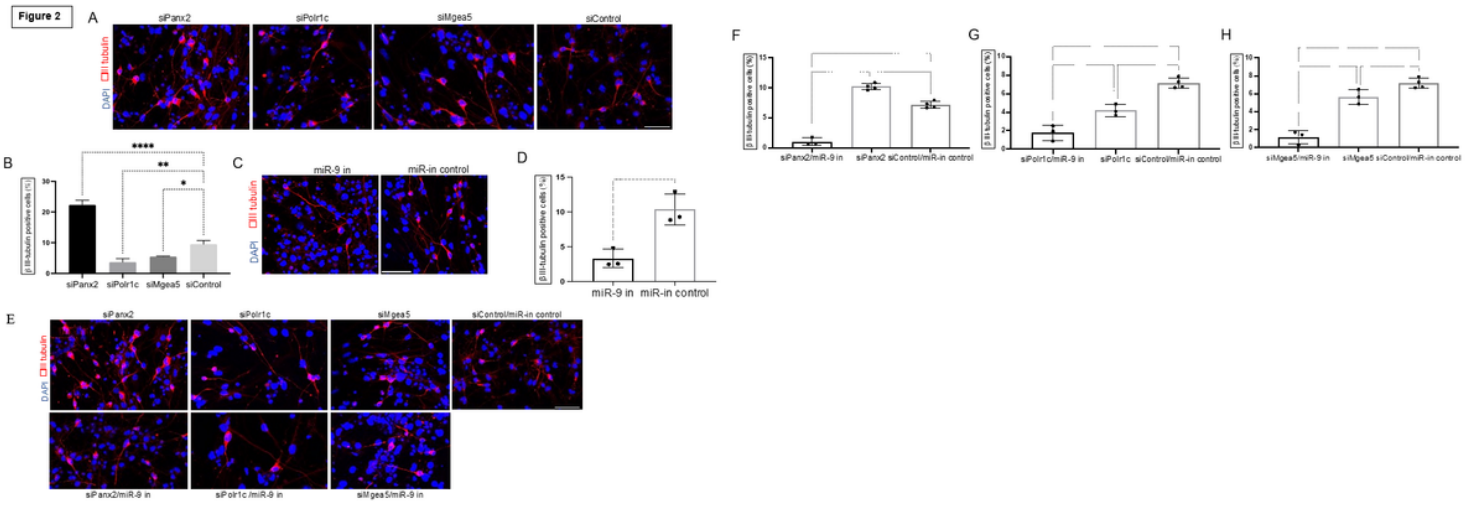

Figure 2

***Panx2*, *Polr1c* and *Mgea5* alter neuronal differentiation through miR-9.**

(A-B) Role of *Panx2*, *Polr1c* and *Mgea5* in neuronal differentiation. Representative images (A) and quantification (B) of βIII-tubulin positive cells using immunostaining in differentiated mNPCs transfected with individual siRNAs and scrambled siRNA negative control.

N= 9 experiments. mean ± SEM, ****p<0.0001, ***p<0.0005, **p<0.005, *p<0.05. One-way Anova. Image scale bars=10 µm.

(C-D) miR-9 inhibits neuronal differentiation in mNPCs. Representative images (C) and quantification (D) of βIII-tubulin positive cells using immunostaining in differentiated mNPCs transfected with miR-9 inhibitor and miR negative control. N=3 experiments. mean ± SEM, **p<0.005. Unpaired T-test. Image scale bars=10 µm.

(E-H) *Panx2*, *Polr1c* and *Mgea5* acts through miR-9 to alter neuronal differentiation. Representative images (E) and quantification (F-H) of βIII-tubulin positive cells using immunostaining in differentiated mNPCs transfected with a combination of individual siRNAs plus miR-9 inhibitor and negative control- (F) siPanx2 plus miR-9 in, (G) siPolr1c plus miR-9 in and (H) siMgea5 plus miR-9 in.

N= 6 experiments. mean ± SEM, ****p<0.0001, ***p<0.0005, **p<0.005, *p<0.05. One-way Anova. Image scale bars=10 µm.

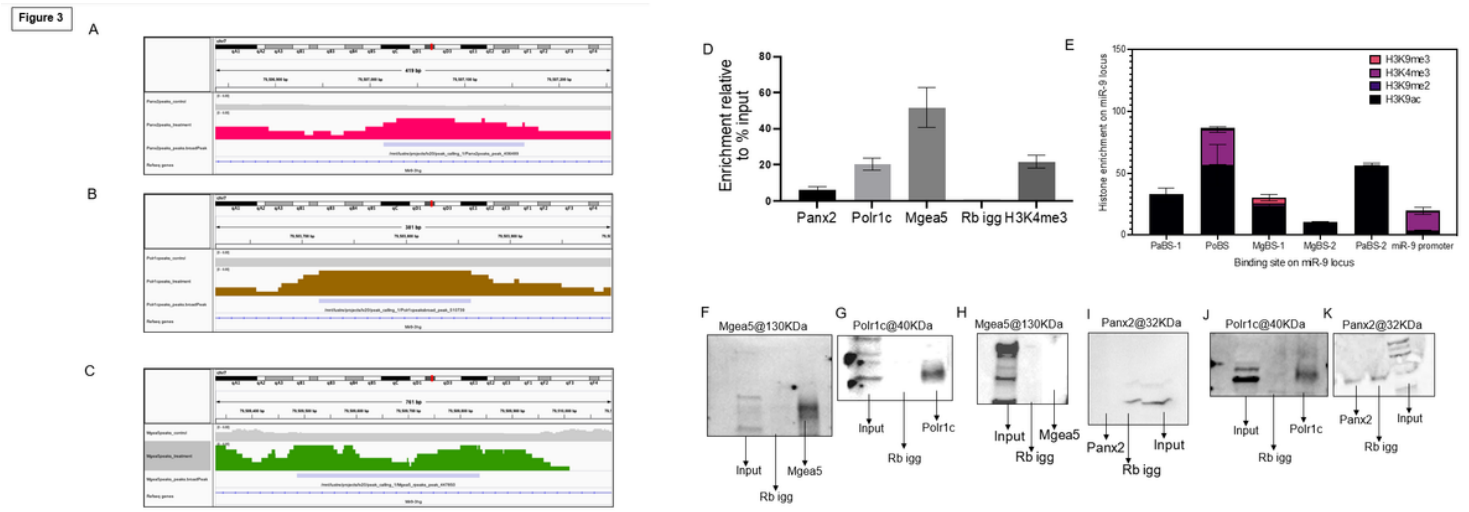

Figure 3

Panx2, Polr1c and Mgea5 are recruited to the miR-9 genomic locus.

(A-C) Panx2 (A), Polr1c (B) and Mgea5 (C) is recruited to the genomic region of miR-9 locus as determined by the ChIP-seq peak analysis using MACS3 software. Peaks were viewed in IGV- Panx2 (Magenta color), Polr1c (Brown color) and Mgea5 (Green color) against the Input control (Gray color).

ChIP-seq experiments were performed in duplicates. The peaks shown in IGV is representative of one experiment.

(D) ChIP-qPCR validation of Panx2, Polr1c and Mgea5 binding to the miR-9 locus. The binding was confirmed against a negative control (Rabbit IgG) which showed no enrichment on the mir-9 locus and a positive control (H3K4me3) which shows prominent enrichment. The enrichment of IP signal for Panx2, Polr1c and Mgea5 was normalized over the Input signal at the selected locus. N=3 experiments, mean ± SEM.

(E) Analysis of chromatin structure was conducted by ChIP-qPCR to assess the histone specific enrichment on the miR-9 locus. The chromatin fragments were immunoprecipitated using antibodies against H3K4me3, H3K9/14ac, H3K9me2 and H3K9me3 across the 34kb miR-9 locus and amplified with qPCR using primer sets for 3C assay. N=3 experiments, mean ± SEM.

(F-K) Co-immunoprecipitations representing (F-G) interactions of Panx2, (H-I) interactions of Polr1c and (J-K) interactions of Mgea5 immunoblotted against each other. The bands in the rabbit igg lane in (4I, 4K) could be due to impurities in the rabbit IgG. Data is shown as a representative from three independent experiments

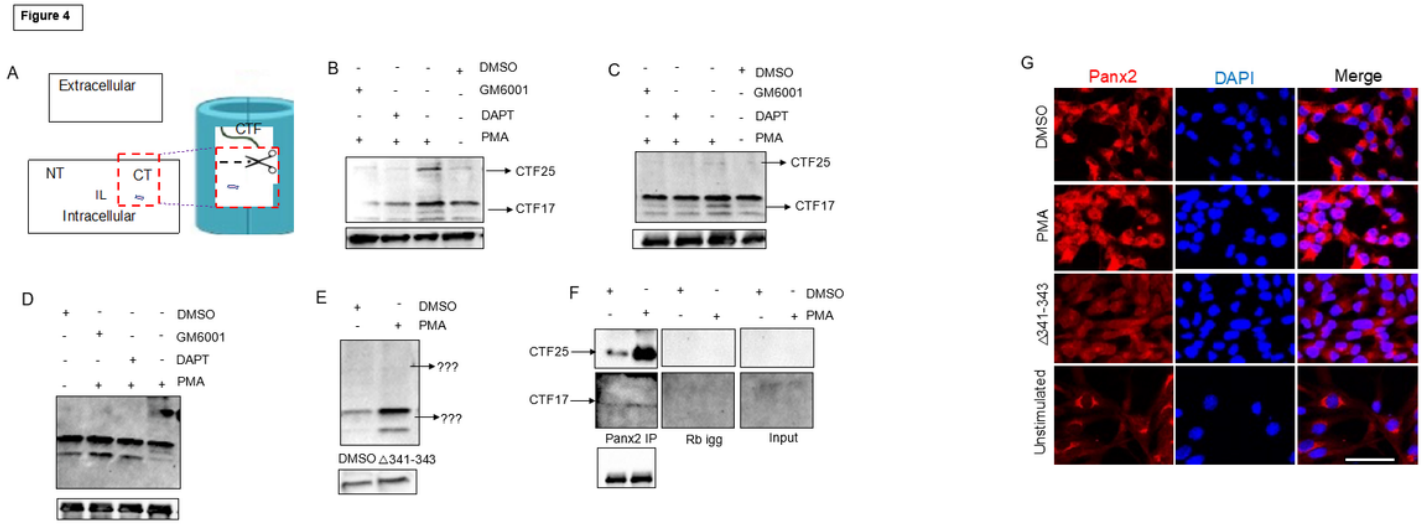

Figure 4

Shedding of Panx2 C-terminal fragment and nuclear translocation.

(A) Schematic of the membrane topology of Panx2. It is a membrane protein having four transmembrane domains, two extracellular loops, one intracellular loop, intracellular amino (NH$_2$) and carboxyl (COOH)

termini.

(B) mNPCs incubated in the presence or absence of PMA, inhibitors (DAPT and GM6001) and vehicle to determine the shedding of Panx2 in a serum-free medium. PMA accelerated the shedding of c-terminal fragment of endogenous Panx2 with two bands at CTF25 and CTF17 whereas these bands were reduced upon inhibition with DAPT and GM6001 as compared to the vehicle as visualised by western blotting against Panx2 antibody.

(C) mNPCs stably expressing Panx2 were also treated with PMA. PMA increased the cleavage of Panx2 CTF showing bands at CTF25 and CTF17. The inhibitors DAPT and GM6001 significantly reduced CTF25 and CTF17 against the vehicle.

(D) mNPCs transfected with Panx2 CTF were also treated with PMA. PMA treatment resulted in enrichment of bands at CTF25 and CTF17. The inhibitors DAPT and GM6001 significantly reduced CTF25 and CTF17 which matched the vehicle control.

(E) mNPCs transiently expressing Panx2 CTF were mutated (at amino acid positions: 341-343) to generate mutant NLS C-terminal sequence. These cells were treated with PMA and compared to the vehicle. The fragments CTF25 and CTF17 were not formed as detected by western blotting.

(F) Nuclear extracts immunoprecipitated with Panx2 CTF antibody showed increased amount of CTF25 after PMA treatment as compared to the vehicle in the mNPCs. Upon overexposure, CTF17 was also observed by the western blot. The rabbit IgG and input control was used as a control.

(G) Immunostaining reveals the transport of Panx2 CTF to the nucleus. mNPCs transiently transfected with mutant CTF and WT mNPCs treated with PMA, vehicle and unstimulated were used. The signal intensity in the nucleus is significantly higher as compared to other conditions and unstimulated. Image scale bars=10 μm.

Data is shown as a representative from three independent experiments.

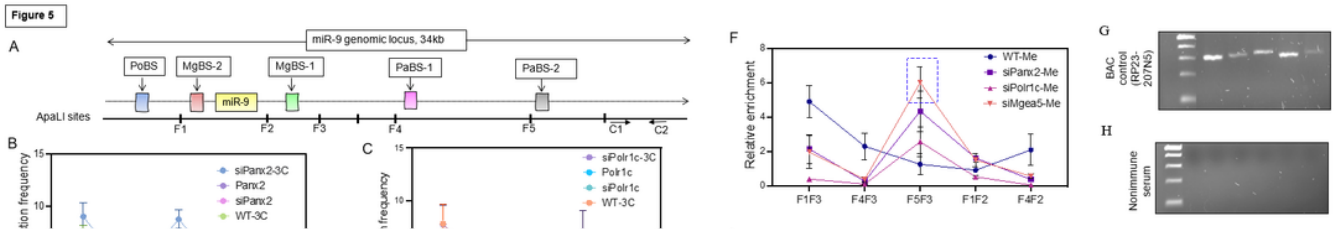

Figure 5

Panx2, *Polr1c* and *Mgea5* form a chromatin associated loop on the miR-9 locus.

(A) 34 kb genomic locus representing *Panx2*/ *Polr1c*/ *Mgea5* binding sites and restriction digestion map of ApaLI across the genomic region with CGBS specific primer pairs (F1-F5).

(B-D) 3C and ChIP-loop assays were done on the 34-kb region containing the miR-9 genomic locus. Crosslinked chromatin was digested with ApaLI and immunoprecipitated with non-immune serum or with antibodies against Panx2, Polr1c or Mgea5. The immunoprecipitated chromatin was diluted in ligation buffer using T4 DNA ligase and was amplified by PCR with various combinations of primers as indicated. 3C indicates chromatin treated as above, except that no immunoprecipitation step was performed. (B) and (C) indicate specific PCR products generated from wild-type chromatin dependant on *Panx2* and *Polr1c* (F2-F4, boxed in red), which were absent in *Panx2*/ *Polr1c* null chromatin. (D) denotes specific PCR product formed in Mgea5 null chromatin (F3-F5, boxed in violet).

(E-F) Crosslinked chromatin was digested with ApaLI, immunoprecipitated against antibodies dimethylated (Me) H3-Lys9 or acetylated (Ac) H3-Lys9/Lys14, ligated, reverse crosslinked and amplified by PCR. F2-F4 interaction gave rise to the enrichment of H3-Lys9/Lys14 which involves acetylation (E) and corresponds to *Panx2*/ *Polr1c* associated chromatin loop. F3-F5 combination showed prominence of H3-Lys9 enrichment which stands for methylation (F) and corresponds to Mgea5 null chromatin.

(G-I) BAC DNA containing the 34-kb miR-9 locus (G) (as positive control), non-immune serum (H) and purified genomic DNA (I) (as negative control) after ApaLI digestion and ligation were used as templates for PCR amplification using various combination of primers shown. (G-I) Lane1: 100bp ladder.

(J) C1 and C2 were used as internal primer control. A1 and A2 indicate PCR products derived from primers from the β-actin locus, used as internal controls for DNA loading, proper ApaLI digestion and

ligation. Lane 1: 100bp ladder; Lane 2: C1-C2 internal control; Lane 3: β-actin locus control

(K) A model of transcription–specific loop organization at the miR-9 genomic locus. This assay identified the *Panx2*/*Polr1c*-associated F2-F4 interaction, with a 8.4-kb intervening chromatin loop, which was absent in Panx2/Polr1c null chromatin. This F2-F4 loop was also associated with chromatin enriched in acetylated (Ac) H3-Lys9/Lys14, suggesting that it is derived from active chromatin. Mgea5-null chromatin had distinctive long-range interaction, such that F3 was associated with F5 forming a 11.2-kb loop. Because F3-F5 interaction was associated with dimethylated (Me) H3-Lys9, these interactions were probably derived from silent chromatin.

All experiments were repeated four to six times, and the data shown were reproducible. Data are represented as mean ± SEM.

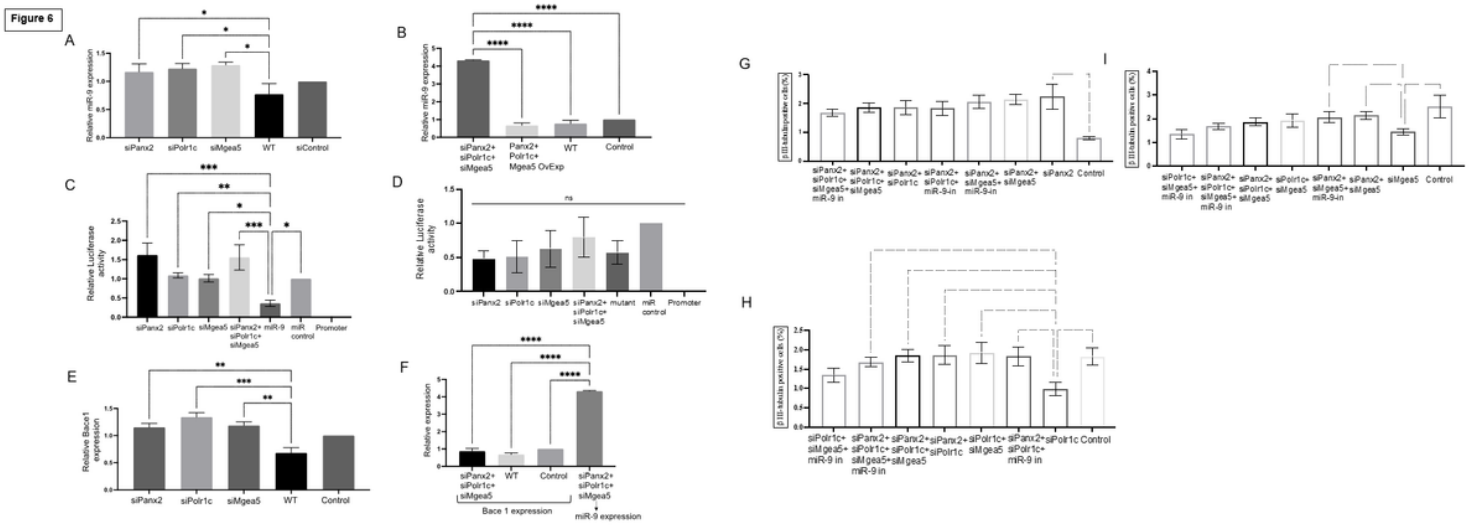

Figure 6

Synergistic effect of miR9Some on miR-9 regulation and neuronal differentiation.

(A) Expression of miR-9 in mNPCs after transfection with *Panx2*, *Polr1c* and *Mgea5* siRNAs. The individual knockdown effect of the three genes was compared to the wild-type mNPCs and negative control (scrambled siRNA).

(B) Combined effect of the miR9Some on miR-9 expression was studied by triple knockdown of miR9Some (*Panx2*/*Polr1c*/*Mgea5*) in mNPCs. A rescue experiment was conducted using lentivirus overexpressing *Panx2*, *Polr1c* and *Mgea5* and miR-9 levels were measured. This data was compared to the wild-type mNPCs and scrambled negative control.

(C-D) Luciferase reporter activity of (C) miR-9 and (D) mutant miR-9 promoter after transfection with *Panx2*, *Polr1c*, *Mgea5* or miR9Some into mNPCs. N= 3 experiments.

(E) Expression of *Bace1* in mNPCs after transfection with *Panx2*, *Polr1c* and *Mgea5* siRNAs. The individual knockdown effect of the three genes was compared to the wild-type mNPCs and negative control

(F) Synergistic effect of the miR9Some on *Bace1* expression was studied by triple knockdown of *Panx2*/ *Polr1c*/ *Mgea5* in mNPCs. This was compared to the wild-type mNPCs and scrambled negative control. *Bace1* and miR-9 expression levels after triple knockdown were matched to establish a regulatory pathway.

(G-I) Synergistic effect of miR9Some on neuronal differentiation was studied by knockdown of (G) *Panx2*, (H) *Polr1c*, (I) *Mgea5* and miR-9 in different combinations. The number of ß tubulin positive cells were quantified in all experiments and compared to individual knockdowns and scrambled negative control.

N= 6 experiments. mean ± SEM, ****p<0.0001, ***p<0.0005, **p<0.005, *p<0.05. One-way Anova.

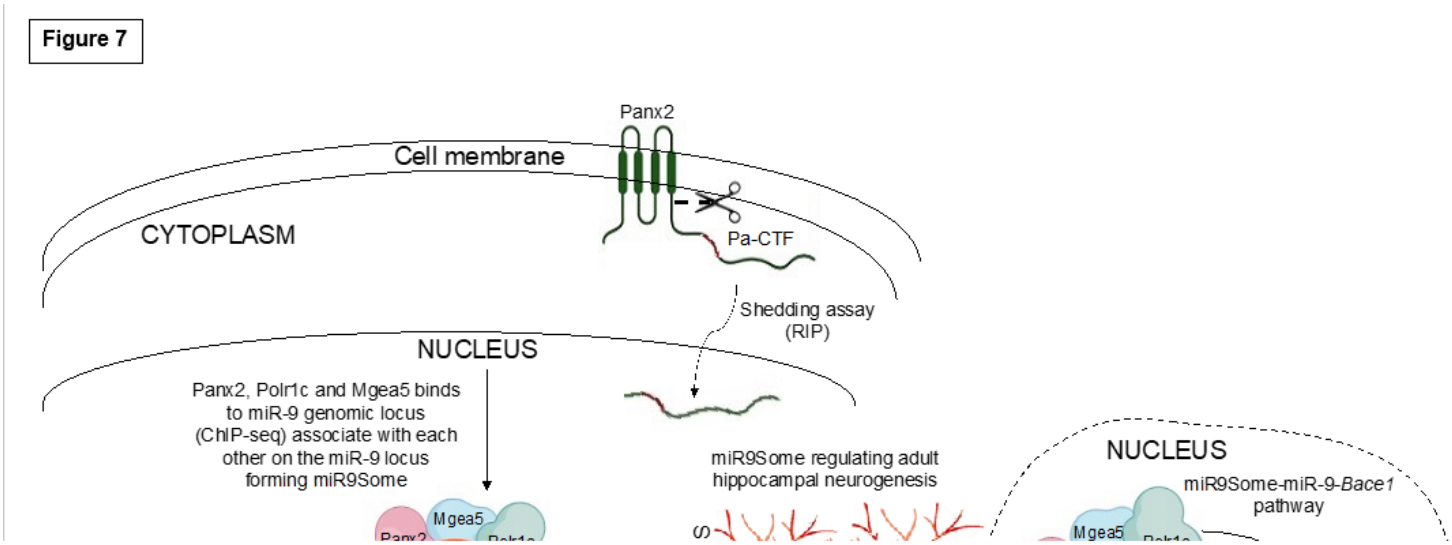

Figure 7

A model of upstream regulation of miR-9 by miR9Some during neurogenesis.

Panx2, a transmembrane protein is cleaved and translocated to the nucleus. In the nucleus, Panx2, Polr1c and Mgea5 bind to the miR-9 locus and associate with each other to form the miR9Some which increases miR-9 expression. miR9Some organises the miR-9 locus into chromatin loops. *Panx2*/*Polr1c* forms acetylation- dependent loops whereas *Mgea5*-null mNPCs form methylation-associated loops. miR9Some null mNPCs upregulates miR-9 expression thereby downregulating *Bace1* levels and increasing neuronal differentiation.

Supplementary Files

This is a list of supplementary files associated with this preprint. Click to download.

- FigureS4MovieG.avi
- FigureS4MovieG.avi
- SupplementalInformation.docx
- SupplementaryFigures.docx